THE JOURNAL OF PHYSICAL CHEMISTRY B

Article

pubs.acs.org/JPCB

Charge, Color, and Conformation: Spectroscopy on Isomer-Selected Peptide Ions

Chang Min Choi,[†] Anne-Laure Simon,[†] Fabien Chirot,[‡] Alexander Kulesza,[†] Geoffrey Knight,[†] Steven Daly,[†] Luke MacAleese,[†] Rodolphe Antoine,[†] and Philippe Dugourd*[,†]

[†]Institut Lumière Matière and [‡]Institut des Sciences Analytiques, Université Lyon 1—CNRS, Université de Lyon, 69622 Villeurbanne Cedex, France

ABSTRACT: Monitoring the chromism induced by intramolecular hydrogen and charge transfers within proteins as well as the isomerization of both protein and cofactor is essential not only to understand photoactive signaling pathways but also to design targeted opto-switchable proteins. We used a dual-ion mobility drift tube coupled to a tunable picosecond laser to explore the optical and structural properties of a peptide chain bound to a chromophore—a prototype system allowing for a proton transfer coupled to conformational change. With the support of molecular dynamics and DFT calculations, we show how proton transfer between the peptide and its cofactor can dramatically modify the optical properties of the system and demonstrate that these changes can be triggered by collisional activation in the gas phase.

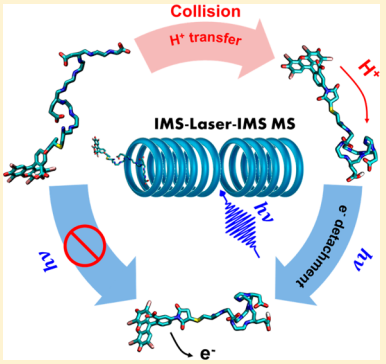

INTRODUCTION

Living cells constantly monitor their own state and their surroundings in order to respond effectively to changes in them. Photoactive signaling pathways rely on proteins with bound organic cofactors providing the possibility to sense light stimuli through cis−trans isomerization—such as in the vision process—or via electron and proton transfer reactions within and between proteins, which eventually trigger a series of biochemical reactions.[1−4] Both charge transfer and mechanical strain exerted by the protein environment can in turn dramatically change the optical properties of chromophores.[5,6]

Thus, monitoring the chromism induced by intramolecular hydrogen and charge transfers as well as the isomerization of the protein and cofactor is essential not only to understand life but also to design targeted photoswitchable proteins.[7−11] Gas-phase experiments with the coupling of laser spectroscopy and ion mobility spectrometry (IMS)[12,13] have recently been used by Bieske and co-workers to provide information on the photoisomerization of charged photoactive molecules.[14,15] The present work parallels such studies in investigating the effects of collisionally activated isomerization on optical properties. It opens a new way to probe opto-switching in proteins despite conformational heterogeneity among different individual copies of the same protein. Herein, we report the first results on a prototype system allowing for a proton transfer coupled to conformational change: an acidic chromophore bound to a negatively charged host peptide. The chromophore is the fluorescein derivative Eosin Y (Eo) maleimide (see Scheme 1), which in solution has three absorption maxima which correspond to different protonation states.[16] The peptide sequence is CAAEAADAA, which was chosen to include several acidic residues to permit proton transfer between the chromophore and the neighboring side chains of the host peptide. In the following Eo−P refers to the chromophore−peptide complex, where the chromophore is covalently bound to the thiol moiety of the cysteine residue. We used a dual-ion mobility drift tube coupled to a tunable picosecond laser to measure the isomer-resolved optical spectroscopy of Eo−P anions to explore how the protonation state of the chromophore and the charged residues of the peptide influence the conformation and optical properties of the complex and how collisional activation can be used to induce changes in those properties. The results are interpreted in light of molecular dynamics and DFT calculations.

MATERIAL AND METHODS

Chemicals. The peptide H−CAAEAADAA−OH was purchased from GeneCust (Luxembourg) and dissolved in H_2O to a concentration of 1.5 mM. Eosin Y maleimide was dissolved in DMSO to a concentration of ∼14 mM. A 15 μL amount of this solution was added to 150 μL of the peptide solution. The resulting solution was left at room temperature for 1 h to achieve Eosin Y maleimide tagging at the N terminus of the peptide. The solution was further diluted to a concentration of ∼10 μM, and 0.1% of NH_4OH was added before electrospray.

Experiment. We used a tandem IMS instrument coupled to a high-resolution time-of-flight mass spectrometer (Figure 1).[17] It consists of two 79 cm long drift tubes (DT1 and DT2) connected by a dual-ion funnel assembly (DF). The arrange-

Received: December 6, 2015
Revised: January 10, 2016
Published: January 12, 2016

DOI: 10.1021/acs.jpcb.5b11919
J. Phys. Chem. B 2016, 120, 709−714

Scheme 1. Chemical Structure for Eo−P[a]

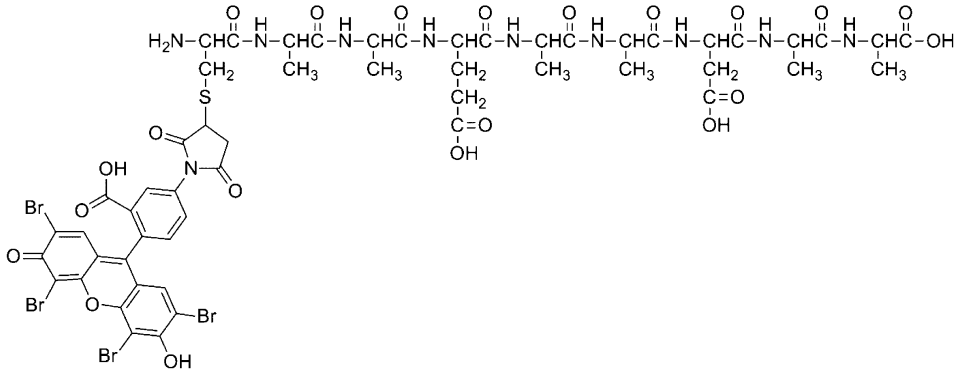

[a]Deprotonation sites are the OH and COOH groups on Eosin Y maleimide, the COOH groups at the side chain of Glu and Asp, and at the C terminus.

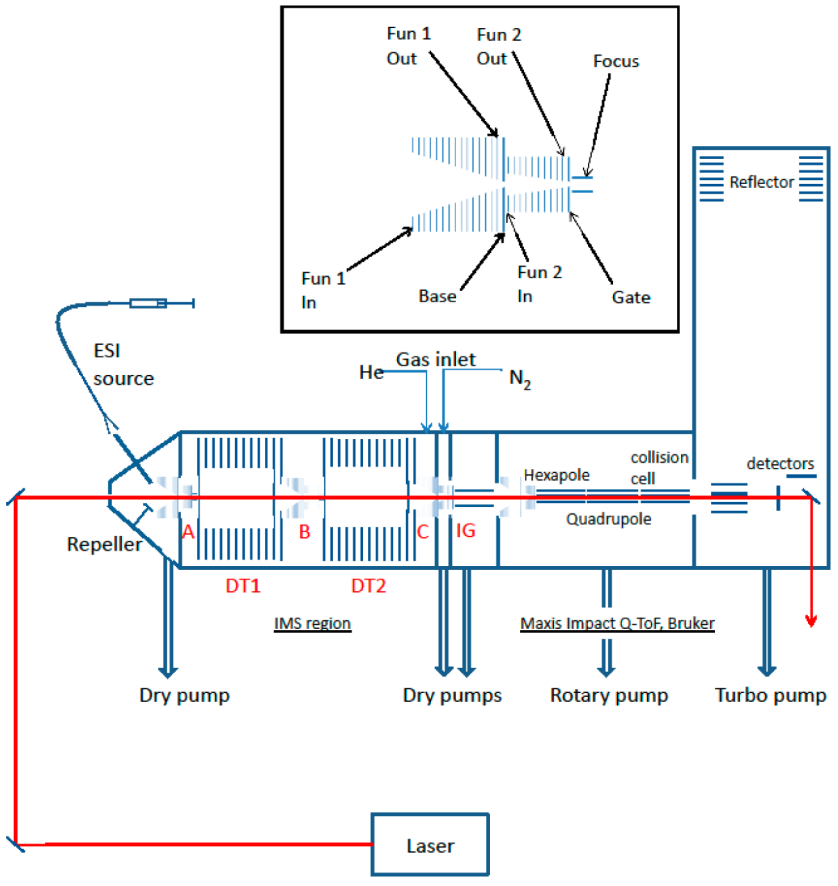

Figure 1. General scheme of the apparatus. The inset details the dual-ion funnel (DF) assembly, denoted A, B, and C on the general scheme. The fourth funnel is the one implemented in the commercial Maxis Impact (Bruker). Laser and collision activations are performed in DF B.

ment allows one to select a particular isomer in a first IMS stage and then irradiate it with a tunable kHz picosecond optical parametric amplifier (PG400, EKPLA, Lithuania), the photoproducts being separated in the second IMS stage before mass analysis. Activation by collisions is possible between the two IMS stages by applying an activation voltage between two electrodes in the middle of the dual-ion funnel. In DT1 and DT2, helium buffer gas is maintained at a pressure of ~4 Torr, the temperature, T, at 300 K, and with typical voltage drops across DT1 and DT2 of 500 V. Experimental collision cross section (CCS) are determined by measuring ion arrival times (AT) as a function of the inverse voltage value across DT2 and by fitting resulting values using eq 1[18]

$$\mathrm{AT} = t_0 + \frac{16}{3}\sqrt{\frac{\mu k_B T}{2\pi}}\frac{\mathrm{NL^2CCS}}{q}\frac{1}{V} \quad (1)$$

with μ being the reduced mass for ion−buffer gas collisions, N the number density of the buffer gas, V the voltage across DT2, and L the drift length. t_0 corresponds to the transfer time of the ions from the end of DT2 to the detector.

Optical action spectra were obtained by irradiating selected ions in DF between DT1 and DT2 and monitoring the

DOI: 10.1021/acs.jpcb.5b11919
J. Phys. Chem. B 2016, 120, 709−714

depletion of these ions as a function of the laser wavelength. The yield of depletion Y at each wavelength is given by

$$\ln\left(\frac{I_0}{I}\right)/\varphi \propto Y \tag{2}$$

where φ is the laser fluence and I_0 and I are the peak intensity without and with laser.

Reference spectra in Figures 3a, 3d, and 4 were recorded similarly but on m/z selected ions using a dual-linear ion trap coupled to nanosecond optical parametric oscillator.[19]

Computational. We modeled the structure of Eosin-functionalized peptides in the gas phase by classical molecular dynamics based on the AMBER99 force field[20,21] within a generalized ensemble approach. We parametrized the Eosin chromophore in different charge and protonation states with the generalized Amber Force Field (GAFF)[22,23] and employed replica-exchange molecular dynamics[24] as implemented in Gromacs 5.0.2[25,26] to access low-energy conformations and generate canonical ensembles (see ref 27 for details). The lowest energy structures were subsequently reoptimized at the DFT level using the hybrid functional CAM-B3LYP[28−30] for exchange and correlation combined with Grimme's empirical dispersion correction including Becke−Johnson damping D3(BJ).[31,32] DFT optimizations employed Ahlrichs split-valence plus polarization basis sets (def2-SVP) on all atoms. Single-point energies were then calculated with a TZVP basis set.[33] We used Gaussian09 Rev D.01[34] for these calculations. Collision cross sections were calculated using an exact hard-spheres scattering model.[35]

RESULTS AND DISCUSSION

A solution of Eo−P (10 μM in H_2O) was injected in negative mode into the electrospray source. Eo−P ions with charge states 5−, 4−, and 3− were observed. We focus on the quadruply charged species, further denoted $[Eo-P]^{4-}$. For tandem-IMS measurements, ions were accumulated and then pulsed into the first drift tube (DT1) at a rate of ∼10 Hz. At the end of DT1, a pulsed ion gate can be used to allow only ions with a specific mobility to pass. The selected ions were then trapped in a dual-ion funnel assembly (DF B in Figure 1) before injection in the second drift tube (DT2). Figure 2d shows the full arrival time distribution (ATD) obtained (without selection) for $[Eo-P]^{4-}$. Three distinct peaks are observed, further denoted A, B, and C, in increasing order of drift time. The corresponding experimental CCS are listed in Table 1.

Isomer-resolved collisional activation experiments were performed on each population of ions by applying a voltage drop between the two stages of the DF, i.e., after selection at the end of DT1 and before injection in DT2.[17] Comparison of the ATDs recorded after DT2 for different activation voltages (Figure 2a−c) allows one to probe interconversions between the different peaks.[36,37] After selection of peak A (Figure 2a), isomerization toward peak B is observed even at low excitation voltage and is amplified at high excitation voltage. After selection of peak B, the reverse process is observed, although more limited (Figure 2b). In this case, the fact that the ratio between peak A and peak B is essentially unaffected by the excitation voltage suggests that thermal isomerization between A and B occurs in DT2 and that the observed distribution reflects the equilibrium between the two populations of structures. When peak C is selected (Figure 2c), isomerization

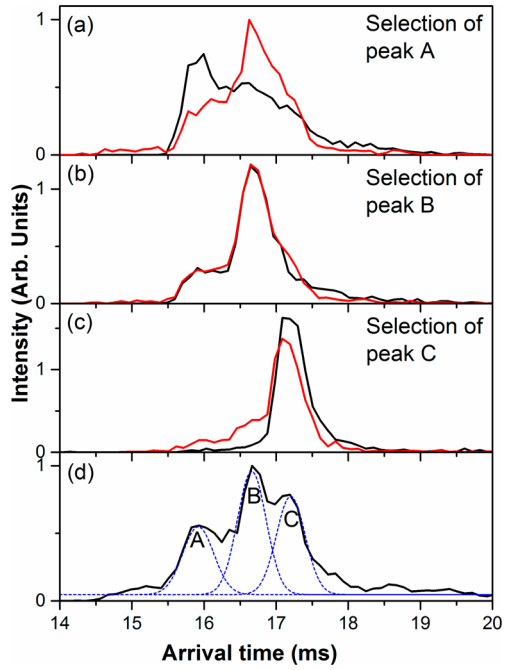

Figure 2. Arrival time distributions (ATDs) recorded for $[Eo-P]^{4-}$ (d). Three peaks are identified and labeled A, B, and C. Results of selection and activation scans, where selection is applied to peak A (a), B (b), and C (c) (black line, excitation voltage 4 V; red line, excitation voltage 74 V); 4 V corresponds to the minimum value required for ion transfer and induces minimal excitation in this region. The curves at different activation energies have been normalized for comparison.

Table 1. Calculated Relative Energies (ΔE) and CCS (calculated for the DFT-optimized structure and averaged over the T = 292 K REMD ensemble) of $[Eo-P]^{4-}$ Compared to the Experimental Values[a]

	ΔE [kJ/mol] DFT structure	CCS [Å^2] DFT structure	CCS [Å^2] REMD, av value 292 K	CCS [Å^2] exp value (peak label)
EoE^HDC_t	0	347	359	382 ± 12 (B)
$EoED^HC_t$	+10	353	356	367 ± 12 (A)
Eo^HEDC_t	+55	387	396	399 ± 10 (C)
$EoEDC_t^H$	+30	374	391	
Eo^-		142		139 ± 3
Eo^{2-}		143		148 ± 3

[a]Peak assignment (see Figure 2d) is given in parentheses. CCS values for doubly and singly charged Eosin Y are given for reference.

is only observed at high activation voltage, leading to peaks B and, to a lesser extent, A. Altogether peak B corresponds to the most stable structures. Spontaneous isomerization between A and B is observed at room temperature, while more energy is required to convert C to A and B.

Optical action spectra for each family of structures were recorded by irradiating the mobility-selected ions in DF B. Peaks A and B were selected together, since they were found to spontaneously interconvert (vide supra). After laser excitation, the main relaxation channel for all species corresponds to electron detachment leading to the formation of a triply negatively charged radical ion.[38] The action spectrum recorded for A and B (Figure 3b) shows a band centered at 510 nm with a shoulder at 475 nm. The detachment yield is much lower for isomer C (Figure 3c), leading to a broad band ranging from

DOI: 10.1021/acs.jpcb.5b11919
J. Phys. Chem. B 2016, 120, 709−714

460 to 540 nm. The origin of the differences between Figure 3b and 3c can be understood with the examination of the action

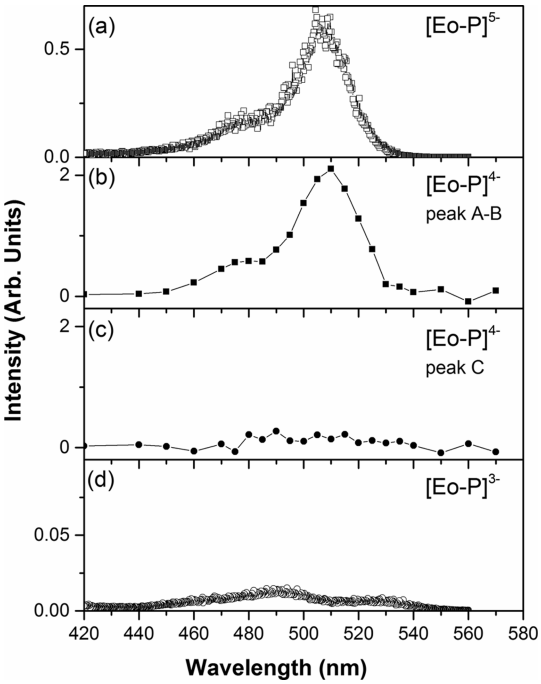

Figure 3. Action spectra recorded for $[Eo-P]^{5-}$ (a), $[Eo-P]^{4-}$ peaks A and B (b), $[Eo-P]^{4-}$ peak C (c), and $[Eo-P]^{3-}$ (d). (b and c) Obtained using the dual-ion mobility setup. ATD for $[Eo-P]^{5-}$ and $[Eo-P]^{3-}$ display a single major peak. A linear ion trap was then used to record spectra in a and d.[19]

spectra recorded for $[Eo-P]^{5-}$ and $[Eo-P]^{3-}$ (Figure 3a and 3d). In $[Eo-P]^{5-}$, the chromophore bears two negative charges while it bears a single charge in $[Eo-P]^{3-}$, as confirmed by spectra recorded for bare Eo^{-} and Eo^{2-} (Figure 4). The similarity between the action spectra recorded for $[Eo-P]^{5-}$ and peaks A and B of $[Eo-P]^{4-}$ and on the other hand for $[Eo-P]^{3-}$ and peak C of $[Eo-P]^{4-}$ suggests that the different optical responses observed in Figure 3c and 3d are due to the different charge state of the chromophore (doubly charged in A

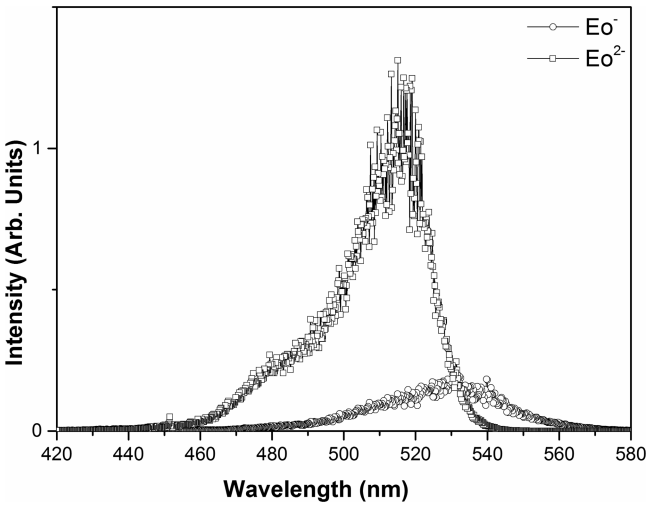

Figure 4. Action spectra recorded for Eo^{-} (circles) and Eo^{2-} (squares).

and B and singly charged in C). The overall Figure 3 suggests that for peaks A and B the Eo moiety is a dianion, while in C it is a monoanion.

Calculated structures for $[Eo-P]^{4-}$ were determined through force-field-based replica exchange molecular dynamics (REMD) calculations, followed by DFT optimizations. The most favorable deprotonation site on Eo−P is the hydroxyl group of Eo[16] and is assumed to be deprotonated in all calculations. The 3 remaining charges were distributed between the 4 other possible sites, namely, the carboxyl groups at the side chains of Glu (E) and Asp (D), on Eo, and at the C terminus (C_t) (see Scheme 1). The four corresponding isomers are named after the position of the carboxyl group which remains protonated. $Eo^{H}EDC_t$ stands for a singly charged Eo and deprotonated Asp, Glu, and C terminus. The 3 other structures correspond to doubly deprotonated Eo with two additional charges on the peptide moiety (i.e., in $EoE^{H}DCt$, Asp residue remains protonated, while Glu and C terminus are deprotonated). Relative DFT energies and calculated CCS for the resulting four lowest energy structures are given in Table 1 and shown in Figure 5. The lowest energy isomer corresponds

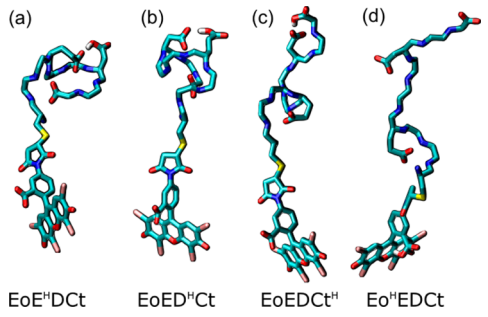

Figure 5. Lowest energy optimized structures for (a) $EoE^{H}DCt$, (b) $EoED^{H}Ct$, (c) $EoEDCt^{H}$, and (d) $Eo^{H}EDCt$ (CH and NH hydrogens, peptide bond oxygens, as well as the Ala side chain omitted for clarity).

to the $EoE^{H}DC_t$ configuration. All configurations with doubly charged Eo lead to structures that are more compact than those with a singly charged Eo ($Eo^{H}EDC_t$). In structures with Eo^{2-}, the protonated carboxyl group can form a hydrogen bond with one of the carboxylates (see Figure 5), which favors proton transfer and subsequent interconversion between the different isomers with Eo^{2-}. When Eo is singly charged, the peptide moieties bear 3 charges and unfold to minimize Coulomb repulsion between these 3 charges, which leads to high CCS. The resulting unfolded configurations do not display favorable structures for proton transfer, contrary to the ones for doubly charged Eo (see Figure 5).

These theoretical results together with Figures 2 and 3 support that Eo is singly charged in peak C, whereas it is doubly charged in peaks A and B. We then assigned $Eo^{H}EDC_t$ to peak C and tentatively $EoE^{H}DC_t$ and $EoED^{H}C_t$ to the two other peaks. According to pK_a values, a distribution of $Eo^{H}EDCt$, $EoE^{H}DCt$, and $EoED^{H}Ct$ is expected for 4− ions in solution. Despite the calculated high relative energy of $Eo^{H}EDCt$ in the gas phase, due to the high isomerization barrier (vide supra) it is possibly kinetically trapped from a solution structure. In this context, the small amount of conformer C that converts toward peaks A and B under collisional activation has undergone proton transfer from the Eo to the peptide moiety. A way to assess the occurrence of such a proton transfer is to measure the effect of light irradiation on the different peaks observed

DOI: 10.1021/acs.jpcb.5b11919
J. Phys. Chem. B 2016, 120, 709−714

after collisional activation. The ions that have experienced proton transfer and then have converted to peaks A and B are expected to be more efficiently photodepleted than ions in peak C. The spectra displayed in Figure 6 correspond to the ATD

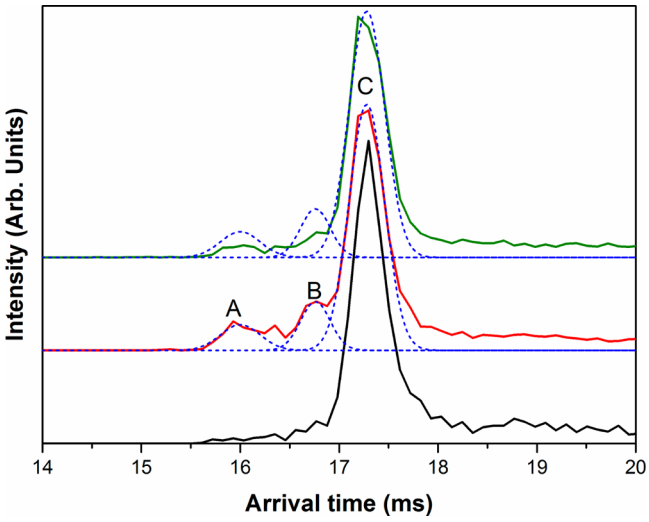

Figure 6. Selection scan ($[Eo-P]^{4-}$ peak C, black line), activation scan (74 V, red line), and activation scan (74 V) with addition of laser irradiation (λ = 520 nm, green line). Laser irradiation is performed in DF after collisional activation. Blue dash lines were fitted on the red curve. They show the population of A, B, and C after activation and before irradiation.

observed after selection of peak C (black line), the ATD obtained after subjecting peak C to collisional activation (red line), and the ATD obtained after subjecting peak C to collisional activation followed by laser excitation at 520 nm (green line). The short-time shoulders, which are observed after collisional excitation and attributed to peaks A and B, are depleted after laser excitation, while the remaining intensity on peak C is very little affected. This is consistent with a switch in the optical response of the system following collision-activated proton transfer (Scheme 2).

Scheme 2. Switch in Photoreactivity Triggered by Collision Activated Proton Transfer

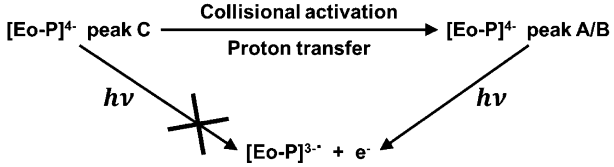

In conclusion, we coupled mass spectrometry, optical spectroscopy, and ion mobility to explore the optical and structural properties of a peptide chain bound to a chromophore—a system with resemblance to blue to red light receptor phototropins, phytochromes, and photoswitchable proteins.[37,39,40] The use of both collision and laser activation in a tandem-IMS scheme allowed us to probe how proton transfer between a peptide and its cofactor can dramatically modify the optical properties of the system. We demonstrated the possibility of collisionally triggering this switch of optical properties. This opens new perspectives for gas-phase structural biology[41,42] with the study of isolated analogous photoswitchable native protein complexes.

AUTHOR INFORMATION

Corresponding Author

*E-mail: phillipe.dugourd@univ-lyon1.fr.

Notes

The authors declare no competing financial interest.

ACKNOWLEDGMENTS

The research leading to these results received funding from the European Research Council under the European Union's Seventh Framework Programme (FP7/2007-2013 Grant agreement No. 320659). A.K. acknowledges COST action BM1403.

REFERENCES

(1) Takala, H.; Björling, A.; Berntsson, O.; Lehtivuori, H.; Niebling, S.; Hoernke, M.; Kosheleva, I.; Henning, R.; Menzel, A.; Ihalainen, J. A.; et al. Signal Amplification and Transduction in Phytochrome Photosensors. *Nature* **2014**, *509*, 245−248.

(2) Christie, J. M.; Blackwood, L.; Petersen, J.; Sullivan, S. Plant Flavoprotein Photoreceptors. *Plant Cell Physiol.* **2015**, *56*, 401−413.

(3) Harper, S. M.; Neil, L. C.; Gardner, K. H. Structural Basis of a Phototropin Light Switch. *Science* **2003**, *301*, 1541−1544.

(4) Schotte, F.; Cho, H. S.; Kaila, V. R. I.; Kamikubo, H.; Dashdorj, N.; Henry, E. R.; Graber, T. J.; Henning, R.; Wulff, M.; Hummer, G.; et al. Watching a Signaling Protein Function in Real Time via 100-Ps Time-Resolved Laue Crystallography. *Proc. Natl. Acad. Sci. U. S. A.* **2012**, *109*, 19256−19261.

(5) Pennacchietti, F.; Losi, A.; Xu, X.; Zhao, K.; Gärtner, W.; Viappiani, C.; Cella, F.; Diaspro, A.; Abbruzzetti, S. Photochromic Conversion in a Red/green Cyanobacteriochrome from Synechocystis PCC6803: Quantum Yields in Solution and Photoswitching Dynamics in Living E. Coli Cells. *Photochem. Photobiol. Sci.* **2015**, *14*, 229−237.

(6) Schäfer, L. V.; Groenhof, G.; Klingen, A. R.; Ullmann, G. M.; Boggio-Pasqua, M.; Robb, M. a.; Grubmüller, H. Photoswitching of the Fluorescent Protein asFP595: Mechanism, Proton Pathways, and Absorption Spectra. *Angew. Chem., Int. Ed.* **2007**, *46*, 530−536.

(7) Lindner, I.; Knipp, B.; Braslavsky, S. E.; Gärtner, W.; Schaffner, K. A Novel Chromophore Selectively Modifies the Spectral Properties of One of the Two Stable States of the Plant Photoreceptor Phytochrome. *Angew. Chem., Int. Ed.* **1998**, *37*, 1843−1846.

(8) Renner, C.; Alefelder, S.; Bae, J. H.; Budisa, N.; Huber, R.; Moroder, L. Fluoroprolines as Tools for Protein Design and Engineering. *Angew. Chem., Int. Ed.* **2001**, *40*, 923−925.

(9) Su, X.; Robbins, T. F.; Aprahamian, I. Switching through Coordination-Coupled Proton Transfer. *Angew. Chem., Int. Ed.* **2011**, *50*, 1841−1844.

(10) Schönberger, M.; Trauner, D. A Photochromic Agonist for μ-Opioid Receptors. *Angew. Chem., Int. Ed.* **2014**, *53*, 3264−3267.

(11) Tsai, Y.-H.; Essig, S.; James, J. R.; Lang, K.; Chin, J. W. Selective, Rapid and Optically Switchable Regulation of Protein Function in Live Mammalian Cells. *Nat. Chem.* **2015**, *7*, 554−561.

(12) Warnke, S.; Baldauf, C.; Bowers, M. T.; Pagel, K.; von Helden, G. Photodissociation of Conformer-Selected Ubiquitin Ions Reveals Site-Specific Cis/trans Isomerization of Proline Peptide Bonds. *J. Am. Chem. Soc.* **2014**, *136*, 10308−10314.

(13) Masson, A.; Kamrath, M. Z.; Perez, M. A. S.; Glover, M. S.; Rothlisberger, U.; Clemmer, D. E.; Rizzo, T. R. Infrared Spectroscopy of Mobility-Selected H+-Gly-Pro-Gly-Gly (GPGG). *J. Am. Soc. Mass Spectrom.* **2015**, *26*, 1444−1454.

(14) Coughlan, N. J. A.; Adamson, B. D.; Gamon, L.; Catani, K.; Bieske, E. J. Retinal Shows Its True Colours: Photoisomerization Action Spectra of Mobility-Selected Isomers of the Retinal Protonated Schiff Base. *Phys. Chem. Chem. Phys.* **2015**, *17*, 22623−22631.

(15) Markworth, P. B.; Adamson, B. D.; Coughlan, N. J. A.; Goerigk, L.; Bieske, E. J. Photoisomerization Action Spectroscopy: Flicking the

DOI: 10.1021/acs.jpcb.5b11919
J. Phys. Chem. B 2016, 120, 709−714

Protonated Merocyanine−spiropyran Switch in the Gas Phase. *Phys. Chem. Chem. Phys.* **2015**, *17*, 25676−25688.
(16) Batistela, V. R.; Pellosi, D. S.; de Souza, F. D.; da Costa, W. F.; de Oliveira Santin, S. M.; de Souza, V. R.; Caetano, W.; de Oliveira, H. P. M.; Scarminio, I. S.; Hioka, N. pKa Determinations of Xanthene Derivates in Aqueous Solutions by Multivariate Analysis Applied to UV−Vis Spectrophotometric Data. *Spectrochim. Acta, Part A* **2011**, *79*, 889−897.
(17) Simon, A.-L.; Chirot, F.; Choi, C. M.; Clavier, C.; Barbaire, M.; Maurelli, J.; Dagany, X.; MacAleese, L.; Antoine, R.; Dugourd, P. Tandem Ion Mobility Spectrometry Coupled to Laser Excitation: IMS Laser IMS. *Rev. Sci. Instrum.* **2015**, *86*, 094101.
(18) Revercomb, H. E.; Mason, E. A. Theory of Plasma Chromatography/Gaseous Electrophoresis- A Review. *Anal. Chem.* **1975**, *47*, 970−983.
(19) Daly, S.; Kulesza, A.; Poussigue, F.; Simon, A.-L.; Choi, C. M.; Knight, G.; Chirot, F.; MacAleese, L.; Antoine, R.; Dugourd, P. Conformational Changes in Amyloid-Beta (12−28) Alloforms Studied Using Action-FRET, IMS and Molecular Dynamics Simulations. *Chem. Sci.* **2015**, *6*, 5040−5047.
(20) Pearlman, D. A.; Case, D. A.; Caldwell, J. W.; Ross, W. S.; Cheatham, T. E.; DeBolt, S.; Ferguson, D.; Seibel, G.; Kollman, P. AMBER, a Package of Computer Programs for Applying Molecular Mechanics, Normal Mode Analysis, Molecular Dynamics and Free Energy Calculations to Simulate the Structural and Energetic Properties of Molecules. *Comput. Phys. Commun.* **1995**, *91*, 1−41.
(21) Wang, J.; Cieplak, P.; Kollman, P. a. How Well Does a Restrained Electrostatic Potential (RESP) Model Perform in Calculating Conformational Energies of Organic and Biological Molecules? *J. Comput. Chem.* **2000**, *21*, 1049−1074.
(22) Wang, J.; Wolf, R. M.; Caldwell, J. W.; Kollman, P. a.; Case, D. a. Development and Testing of a General Amber Force Field. *J. Comput. Chem.* **2004**, *25*, 1157−1174.
(23) Wang, J.; Wang, W.; Kollman, P. A.; Case, D. A. Antechamber, An Accessory Software Package For Molecular Mechanical Calculations. *J. Comput. Chem.* **2005**, *25*, 1157−1174.
(24) Sugita, Y.; Okamoto, Y. Replica-Exchange Molecular Dynamics Method for Protein Folding. *Chem. Phys. Lett.* **1999**, *314*, 141−151.
(25) Van Der Spoel, D.; Lindahl, E.; Hess, B.; Groenhof, G.; Mark, A. E.; Berendsen, H. J. C. GROMACS: Fast, Flexible, and Free. *J. Comput. Chem.* **2005**, *26*, 1701−1718.
(26) Hess, B.; Kutzner, C.; van der Spoel, D.; Lindahl, E. GROMACS 4: Algorithms for Highly Efficient, Load-Balanced, and Scalable Molecular Simulation. *J. Chem. Theory Comput.* **2008**, *4* (3), 435−447.
(27) Kulesza, A.; Daly, S.; MacAleese, L.; Antoine, R.; Dugourd, P. Structural Exploration and Förster Theory Modeling for the Interpretation of Gas-Phase FRET Measurements: Chromophore-Grafted Amyloid-β Peptides. *J. Chem. Phys.* **2015**, *143*, 025101.
(28) Becke, A. Density Functional Thermochemistry III The Role of Exact Exchange. *J. Chem. Phys.* **1993**, *98*, 5648−5652.
(29) Perdew, J.; Burke, K.; Ernzerhof, M. Generalized Gradient Approximation Made Simple. *Phys. Rev. Lett.* **1996**, *77*, 3865−3868.
(30) Yanai, T.; Tew, D. P.; Handy, N. C. A New Hybrid Exchange-Correlation Functional Using the Coulomb-Attenuating Method (CAM-B3LYP). *Chem. Phys. Lett.* **2004**, *393*, 51−57.
(31) Grimme, S.; Ehrlich, S.; Goerigk, L. Effect of the Damping Function in Dispersion Corrected Density Functional Theory. *J. Comput. Chem.* **2011**, *32*, 1456−1465.
(32) Grimme, S.; Antony, J.; Ehrlich, S.; Krieg, H. A Consistent and Accurate Ab Initio Parametrization of Density Functional Dispersion Correction (DFT-D) for the 94 Elements H-Pu. *J. Chem. Phys.* **2010**, *132*, 154104.
(33) Weigend, F.; Ahlrichs, R. Balanced Basis Sets of Split Valence, Triple Zeta Valence and Quadruple Zeta Valence Quality for H to Rn: Design and Assessment of Accuracy. *Phys. Chem. Chem. Phys.* **2005**, *7*, 3297−3305.
(34) Frisch, M. J.; Trucks, G. W.; Schlegel, H. B.; Scuseria, G. E.; Robb, M. A.; Cheeseman, J. R.; Scalmani, G.; Barone, V.; Mennucci, B.; et al. *Gaussian 09*, Revision D.01; Gaussian Inc.: Wallingford, CT, 2009.
(35) Shvartsburg, A. A.; Jarrold, M. F. An Exact Hard-Spheres Scattering Model for the Mobilities of Polyatomic Ions. *Chem. Phys. Lett.* **1996**, *261*, 86−91.
(36) Shi, H.; Atlasevich, N.; Merenbloom, S. I.; Clemmer, D. E. Solution Dependence of the Collisional Activation of Ubiquitin [M + 7H](7+) Ions. *J. Am. Soc. Mass Spectrom.* **2014**, *25*, 2000−2008.
(37) Dilger, J.; Musbat, L.; Sheves, M.; Bochenkova, A. V.; Clemmer, D. E.; Toker, Y. Direct Measurement of the Isomerization Barrier of the Isolated Retinal Chromophore. *Angew. Chem., Int. Ed.* **2015**, *54*, 4748−4752.
(38) Antoine, R.; Dugourd, P. Visible and Ultraviolet Spectroscopy of Gas Phase Protein Ions. *Phys. Chem. Chem. Phys.* **2011**, *13*, 16494−16509.
(39) Corchnoy, S. B.; Swartz, T. E.; Lewis, J. W.; Szundi, I.; Briggs, W. R.; Bogomolni, R. A. Intramolecular Proton Transfers and Structural Changes during the Photocycle of the LOV2 Domain of Phototropin 1. *J. Biol. Chem.* **2003**, *278*, 724−731.
(40) Toh, K. C.; Stojkovic, E. A.; van Stokkum, I. H. M.; Moffat, K.; Kennis, J. T. M. Proton-Transfer and Hydrogen-Bond Interactions Determine Fluorescence Quantum Yield and Photochemical Efficiency of Bacteriophytochrome. *Proc. Natl. Acad. Sci. U. S. A.* **2010**, *107*, 9170−9175.
(41) Rosati, S.; Rose, R. J.; Thompson, N. J.; van Duijn, E.; Damoc, E.; Denisov, E.; Makarov, A.; Heck, A. J. R. Exploring an Orbitrap Analyzer for the Characterization of Intact Antibodies by Native Mass Spectrometry. *Angew. Chem., Int. Ed.* **2012**, *51*, 12992−12996.
(42) Marcoux, J.; Robinson, C. V. Twenty Years of Gas Phase Structural Biology. *Structure* **2013**, *21*, 1541−1550.

DOI: 10.1021/acs.jpcb.5b11919
J. Phys. Chem. B 2016, 120, 709−714